Combined high alkalinity and pressurization enable efficient CO2electroreduction to CO

Christine M. Gabardo, Ali Seifitokaldani, Jonathan P. Edwards, Cao-Thang Dinh, Thomas Burdyny, Golam Kibria, Colin P. O'Brien, Edward H. Sargent, and David Sinton

Combined high alkalinity and pressurization enable efficient CO_2 electroreduction to CO

Christine M. Gabardo,[†a] Ali Seifitokaldani,[†b] Jonathan P. Edwards,[†a] Cao-Thang Dinh,[b] Thomas Burdyny,[a,c] Md Golam Kibria,[b] Colin P. O'Brien,[a] Edward H. Sargent [b] and David Sinton [a]

The electroreduction of CO_2 to CO is a promising strategy to utilize CO_2 emissions while generating a high value product. Commercial CO_2 electroreduction systems will require high current densities (>100 mA/cm^2) as well as improved energetic efficiencies (EEs), achieved via high CO selectivity and lowered applied potentials. Here we report a silver-based system that exhibits the lowest overpotential among CO_2-to-CO electrolyzers operating at high current densities, 300 mV at 300 mA/cm^2, with near unity selectivity. We achieve these improvements in voltage efficiency and selectivity via operation in a highly alkaline reaction environment (which decreases overpotentials) and system pressurization (which suppresses the generation of alternative CO_2 reduction products), respectively. In addition, we report a new record for the highest half-cell EE (>80%) for CO production at 300 mA/cm^2.

Introduction

In light of worldwide goals of reducing CO_2 emissions, CO_2 utilization has grown into a global and accelerated effort.[1–3] The electrochemical carbon dioxide reduction reaction (CO_2RR) has gained attention due to its potential to sequester up to an estimated 10% of anthropogenic CO_2 emissions into chemical products synthesized utilizing renewable energy sources.[4–6] A wide variety of products can be produced from CO_2RR by varying the catalyst, reaction environment, and operating potential. Carbon monoxide (CO) is a versatile feedstock for various chemicals and fuels and is viewed as having a promising value and market size, making it a first commercial target of interest.[7] Technoeconomic assessment has shown that CO is among the products which have the potential to achieve positive gross margins from CO_2 electroreduction.[7]

A commercial CO_2RR system will require current densities between 100-1000 mA/cm^2 to cover the capital expenditures of system.[7–9] The operating costs of the system will be then dictated by the electricity consumption, and this is determined by the energy efficiency (EE) of the system.[6,10] EE is the product of the voltage efficiency (VE) and the Faradaic efficiency (FE) for CO. Consequently, achieving high EE while operating at relevant current densities is crucial to make CO_2RR economically viable.[11] While high FEs have been reported for CO production, the achievement of high EEs has been limited by large cathodic overpotentials, which have exceeded 400 mV,[12–17] lowering the VE when operating at current densities of hundreds of mA/cm^2.[18] In commercial water-splitting electrolysis, typical EEs are above 70%: we conclude that further improvements in VE and EE will be required on path to commercial CO_2RR systems.[9]

Low overpotentials for both half reactions are vital to attain a high full cell VE for CO_2RR. The anodic reaction, generally the well-established oxygen evolution reaction (OER), has sluggish kinetics leading to considerable overpotentials.[19,20] As compared to acidic conditions, it is advantageous to operate OER in alkaline environments as higher efficiencies have been realized and the catalysts employed are earth-abundant Ni-based materials, rather than expensive rare metals.[21–25] One way to simplify cell design is to operate both halves of the cell under similar alkaline environments. Optimizing CO_2RR under alkaline conditions will additionally allow for an easier transition to industrial application, as alkaline electrolyzers are commercially established.

Using alkaline electrolytes at the cathode, such as KOH, would provide additional benefits to cell operation. For instance, the competing hydrogen evolution reaction (HER) is suppressed in alkaline conditions. Furthermore, the high conductivity of a KOH electrolyte would reduce ohmic losses that would otherwise be prohibitively large in the case of more neutral $KHCO_3$ electrolytes, a commonly used electrolyte in CO_2RR.[26,27] For example, use of KOH, at concentrations ranging between 0.5 to 3 M, has shown promise to increase current densities at fixed cell potentials.[15] Finally, at high current densities rapid proton consumption and water-splitting during CO_2RR would inevitably drive up the local pH of more neutral electrolytes during operation, motivating efforts to start from high bulk pH conditions to test CO_2RR stability and performance.

A major step forward in CO_2RR systems came with the incorporation of gas diffusion electrodes (GDEs) in flow cell systems, allowing users to operate in alkaline environments at industrially relevant current densities.[12,15,16,28] GDE flow cell systems have typically been studied under ambient conditions, with only a small number of reports in the literature of pressurized flow cells.[29,30] However, feedstock CO_2 will ultimately be pressurized for ease of transportation,[31,32] supporting the need to thoroughly study these systems under pressurized conditions; similarly, downstream processing of CO by itself,[33] or in a syngas mixture,[34,35] also requires product at elevated pressures.

Here, we first explore the operation of a promising CO_2RR catalyst under highly-alkaline conditions conducive to efficient whole cell operation. We demonstrate unexpected gains in electrode kinetics and overpotential operating in this largely unexplored extreme alkalinity regime. However, the selectivity for CO is altered under these operating conditions. We investigate the selectivity switching mechanism, finding a route to shutdown alternative CO_2RR pathways and improve CO selectivity by the addition of pressure. Through the combination of pressurization and highly-alkaline reaction environments, we achieve the highest half-cell EE for stable CO production at industrially relevant currents.

Results and discussion

Effect of hydroxide concentration on enhancing reaction potentials and kinetics

The effects of extreme electrolyte alkalinity on the voltage characteristics and reaction kinetics of an Ag electrode operating under CO_2 reducing conditions were studied utilizing different concentrations of aqueous potassium hydroxide (KOH) electrolyte: 1, 5, and 10 M. In order to carry out CO_2RR under these extreme alkaline conditions, the electrochemical reaction was conducted in a flow cell system (Fig. S1) using a gas diffusion layer. A 100 nm thick Ag catalyst was deposited through evaporation onto the carbon gas diffusion layer to produce the cathode. This configuration, in which the catalyst layer is positioned directly adjacent to the interface of the CO_2 gas and liquid electrolyte streams, allows for the continuous diffusion of CO_2 to the catalyst layer, even under alkaline conditions. When the system is operated under a continuous stream of CO_2, we observed that the onset potential for current shifted to less negative values as the concentration of KOH was increased. A difference in onset potential between 1 M and 10 M KOH was measured to be approximately 240 mV (Fig. 1(a)). The onset potential for current in 10 M KOH is observed to be -0.117 V vs. a Reversible Hydrogen Electrode (RHE), slightly larger than the thermodynamic potential for CO, -0.109 V vs.

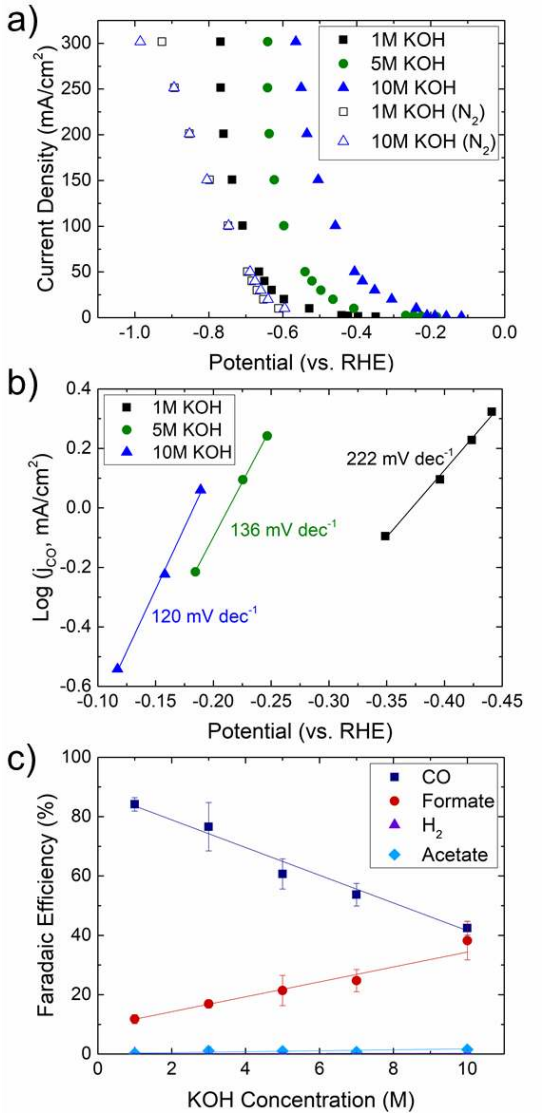

Fig 1. Effect of hydroxide on reaction voltage, kinetics, and product selectivity. a) Current/voltage characteristics of Ag catalyst in 1, 5, and 10 M KOH under CO_2 and N_2 streams. b) Tafel slopes for the CO partial current density (j_{CO}) in 1, 5, and 10 M KOH electrolyte. c) The FE for each CO_2RR product at various concentrations of KOH electrolyte. Error bars indicate the standard deviation of measurements from n≥3 separate samples.

RHE. However, when we operated the system under a nitrogen (CO_2-free) stream, we found that the onset potentials for the hydrogen evolution reaction (HER) for 1 M and 10 M KOH were almost identical at -0.61 V and -0.59 V vs. RHE, respectively. The large difference in onset potential of current operated under CO_2 streams and the onset potential of HER in 10 M KOH, over 400 mV, indicates that our selectivity towards CO_2RR products should be very high, with little competition from HER even at high current densities. Because the potentials reported here are corrected for ohmic losses, the observed voltage differences between the electrolyte concentration are not attributed to increased conductivity, and compensated pH differences would only account for a 59 mV/pH shift in potential, significantly lower than the ~240 mV observed here. Therefore, this substantial potential shift due to KOH concentration in the presence of CO_2 suggests hydroxide molecules have a direct impact on the energy barrier of the CO_2RR product formation.

To study the kinetics of CO_2RR in this system, we obtained Tafel slopes for the CO_2RR current density attributed to CO production (j_{CO}). The slopes were measured to be 222 mV dec^{-1}, 136 mV dec^{-1}, and 120 mV dec^{-1}, for 1 M, 5 M, and 10 M KOH electrolyte respectively (Fig. 1(b)). The decreasing Tafel slope values with increasing KOH concentration indicates that faster kinetics are achieved at the higher hydroxide concentrations.

CO_2 reduction product selectivity as a function of hydroxide concentration

Both VE and FE need to be maximized to achieve high values of EE (see SI for calculation description). With the significantly decreased CO_2 reduction overpotential resulting from the increased KOH concentration (Fig. 1a), the VE of our system was near-unity at low current densities. Next, to assess our overall energy efficiency we measured the reaction selectivity towards CO under various concentrations of KOH while operating in galvanostatic mode at 300 mA/cm^2, a reasonable commercial current density.[10] At 1 M KOH the FE for CO was approximately 84%, leading to a partial current density of CO of 252 mA/cm^2 (Fig. 1(c)). However, as the KOH concentration was increased, this unexpectedly led to a decrease in the FE for CO, with 10 M KOH resulting in only 42% CO. This decrease in selectivity for CO was linked to an increased FE contribution from formate, up to 38% in 10 M KOH from 11% in 1 M KOH when the liquid products were analyzed. Also, as the product selectivity shifted towards more formate production, the total product FE decreased below 100%. We attribute this decrease to unaccounted for formate, which has diffused through the anionic exchange membrane and is either present in the anolyte (2% FE confirmed through liquid product analysis) or has been oxidized at the anode.

Catalyst materials characterization before and after CO_2RR

With the decreased overpotential, increased kinetics, and product selectivity shift, it is reasonable to hypothesize that the structure of the catalyst is altered under the extremely alkaline environment and/or under CO_2RR operation.[36] In order to investigate this hypothesis, materials characterization was performed on the as-made catalyst before CO_2RR, after CO_2RR in 1 M KOH, and after CO_2RR in 10 M KOH. Scanning electron micrographs (SEM) reveal a porous film made up of agglomerated nanoparticles on top of the carbon gas diffusion layer (Fig. S2), ranging in size between ten and several hundred nanometers, with identical morphologies before and after reaction (Fig. 2 (a)). In addition, high resolution transmission electron micrographs (TEM) reveal polycrystalline nanoparticles of similar sizes before and after CO_2RR (Fig. S2). Therefore, the morphology of catalyst did not vary under the reduction and highly alkaline conditions.

Although the morphology did not appear to be altered under CO_2RR, the catalyst could be altered in terms of crystal structure or oxidation state, thus, further materials characterization was required to study these parameters. X-ray absorption spectroscopy (XAS) was then performed to quantify the chemical environment and short-range order of the silver. The Ag K-edge extended X-ray absorption fine structure (EXAFS) spectra (Fig. 2(b)) show that the samples before reaction and after reaction in different KOH concentrations were identical to the reference Ag foil, indicating no change to the oxidation state from Ag^0. Fourier transforms (FT) of the Ag K-edge EXAFS spectra (Fig. S3(a)) revealed a single intense peak arising from the first coordination shell matching the Ag-Ag interaction of Ag foil. All samples showed no evidence of any oxide formation. In addition, L3-edge EXAFS spectra before and after CO_2RR were identical, in agreement with the conclusions from the K-edge spectra (Fig. S3(b)). The Ag peak present in the X-ray photoelectron spectroscopy (XPS) (Fig. 2(d)) did not shift after CO_2RR in both 1 M and 10 M KOH, indicating no surface oxidation state change. Likewise, the X-ray diffraction (XRD) characterization (Fig. 2(c)) showed similar peaks, and by extension, similar crystal phase for all three catalysts.

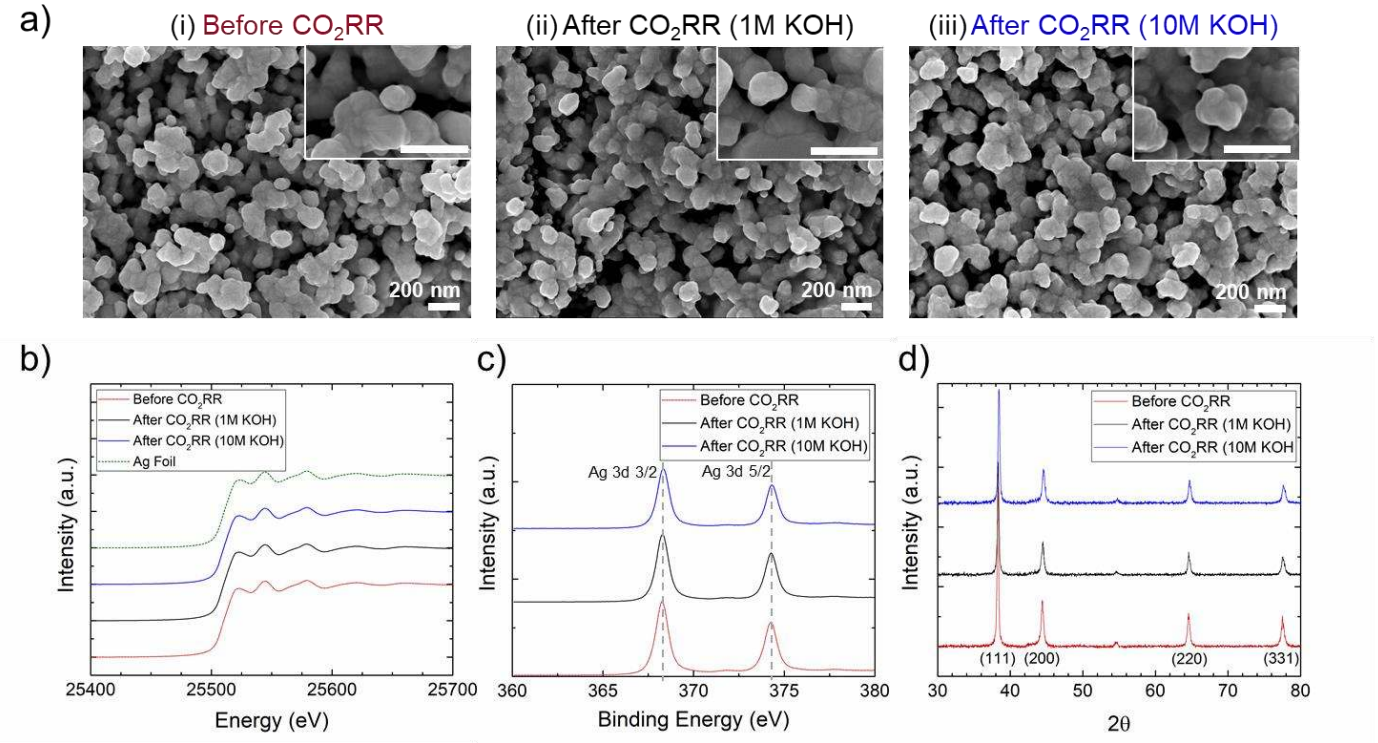

Fig 2. Catalyst materials characterization before and after CO_2RR reaction. a) SEM images of Ag catalyst i) before CO_2RR, ii) after CO_2RR in 1 M KOH, and iii) after CO_2RR in 10 M KOH, with insets displaying higher magnification images with the scale bar representing 200 nm. b) K-edge EXAFS spectra before CO_2RR, after CO_2RR in 1 M KOH, after CO_2RR in 10 M KOH, and Ag foil. c) XPS spectra before CO_2RR, after CO_2RR in 1 M KOH, and after CO_2RR in 10 M KOH. d) XRD spectra before CO_2RR, after CO_2RR in 1 M KOH, after CO_2RR in 10 M KOH.

From this characterization data we can conclude that the silver catalyst did not appear to alter in structure with CO_2RR, remaining stable in morphology, crystalline structure, and oxidation state. Moreover, spray-coated commercial Ag nanoparticles (Fig. S4) were also tested as the catalyst for CO_2RR under 1 M KOH and 10 M KOH electrolytes. Again, a decreased FE for CO and increased FE for formate was observed for the Ag nanoparticle catalyst in 10 M KOH, further indicating that this product selectivity switch in highly alkaline electrolytes is not unique to our Ag catalyst. We therefore attribute the change in catalyst behaviour with varying electrolyte concentrations to the reaction environment of the catalyst, rather than the catalyst itself. Further, we ensured that formate was not produced from a non-CO2 reaction by measuring the products of the evaporated Ag catalyst streams of N2 gas (Fig. S5). Under these conditions, only hydrogen was evolved, and no formate was detected, suggesting that the formate observed under CO2 streams is a product from CO2RR.

As noted in our recent density functional theory work, the increased formate production in highly alkaline environments may be due to a reduced ability for a temporary hydronium molecule to assist in the first protonation step of the *COOH intermediate on the CO reaction pathway, resulting in increased formate production.[37] Further modifications to the local reaction environment that promote CO formation are then of interest provided the observed beneficial reaction kinetics of the highly-alkaline media are maintained.

Pressurization effects on CO_2RR selectivity and efficiency

One of the primary factors determining CO_2RR product selectivity on different catalysts is the relative surface coverage and binding energies of adsorbed protons and CO_2 reduction intermediates.[38–40] Altering the partial and absolute pressures of the CO_2 gas and liquid electrolyte influences this balance, providing an environmental means of altering product selectivity while acting as an industrially relevant parameter for large-scale processes. As such, the system pressure was increased to 3, 5, and 7 atm using a modified flow cell setup (Fig. S6) while operating the Ag catalyst at the previous conditions of 1 M, 5 M, 7 M, and 10 M KOH at a current density of 300 mA/cm^2 (Fig. 3).

The CO selectivity, in terms of FE, was observed to increase with pressure for all concentrations as shown in Fig. 3(a). This increase in CO selectivity is similar to other examples of pressurized silver catalysts in other electrolytes where the CO selectivity was able to reach 85% when pressures of 15 – 30 atm were applied.[14,17,29,30] Compared to these reports, our experiments reach higher selectivities at much lower pressures. In the 10 M KOH electrolyte, the CO faradaic efficiency climbed from 42% at 1 atm to 86% at 7 atm. Similarly, in 7 M KOH the selectivity climbed from 54% to near 100% over the same pressure range. The CO selectivity of the 1 M and 5 M KOH electrolytes plateaued at 5 atm and 7 atm, respectively, at which point they made nearly 100% CO. The inverse trend is observed in Fig. 3(b), wherein the formate selectivity for all electrolyte concentrations is reduced with increased pressurization. At 1 atm 7 M and 10 M KOH, produced substantial quantities of formate, 24.8% and 38.2%, respectively; whereas at 7 atm, the formate selectivity was reduced to 4.4% and 12.0%, respectively.

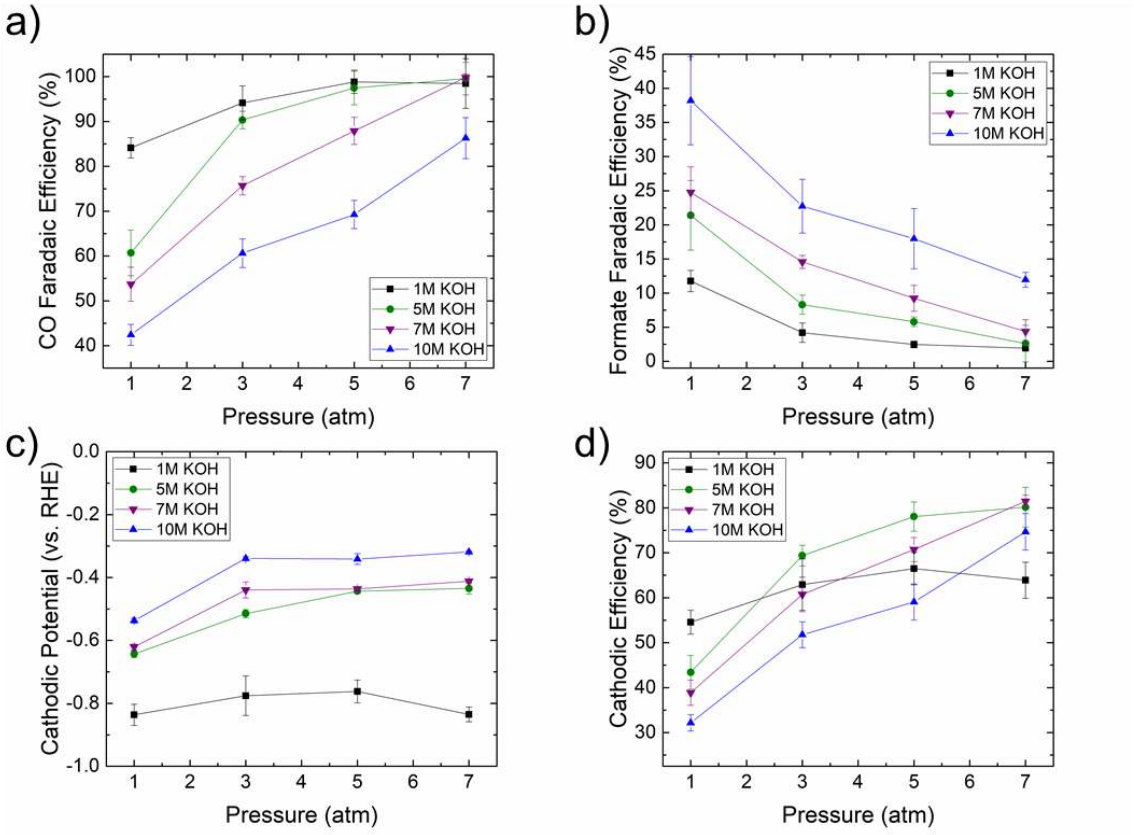

Fig 3. Effect of pressure on CO_2RR at 300mA/cm^2 at various pressures and KOH concentrations. Faradaic efficiency for a) CO and b) formate. The c) cathodic voltage (iR corrected) and corresponding d) cathodic efficiency.

The reason for the shift in selectivity with the application of pressure within these systems is not immediately clear, although three hypotheses were formed. Increasing pressure is known to increase CO_2 surface coverage, and consequently, this leads to a reduction in the number of protons adsorbed on the catalyst surface. The first hypothesis stems from the reduced proton coverage on the surface of the catalyst.[14] Our previous study has demonstrated that direct protonation from adsorbed hydrogen on the surface favors formate production; whereas, if the proton is instead provided by the solution in form of a hydronium ion, then CO is the preferred product.[37] Secondly, the selectivity switch may be due to the increased CO_2 surface coverage. It has been suggested that there are alternate reaction pathways in non-aqueous electrolytes that favor CO over formate production, which

utilize two CO_2 molecules in the rate determining step.[41,42] An increased concentration of CO_2 on the catalyst due to the increase in pressure could lead to the reaction switching to such a pathway. Thirdly, it is possible that the increase in pressure is locally changing the environment around the catalyst to become less basic due to increased CO_2 uptake into the electrolyte. However, our models do not show a significant change in OH^- concentration with pressure (Fig. S7). Of the above three hypotheses, we posit that the first and second, or a combination thereof, are most plausible.

The cathode voltage at 300 mA/cm^2 was monitored for each electrolyte and pressure tested (iR corrected displayed in Fig. 3(c), non-iR corrected cathode and full cell voltage displayed in Fig. S8(a) and Fig. S8(c), respectively). For all electrolyte concentrations, the overpotentials were reduced by approximately 0.2 V from 1 to 3 atm, followed by smaller reductions with subsequent increases in pressure in most cases. The 7 M and 10 M electrolytes corrected cathode voltages improved from -0.62V and -0.53V *vs.* RHE at 1 atm to -0.41V and -0.32 *vs.* RHE at 7 atm, respectively. These voltages correspond to overpotentials of 510 mV and 300 mV for 7 M KOH at 1 and 7 atm, respectively. The voltage of the 1 M electrolyte did not fluctuate substantially from its original value of -0.84 V *vs.* RHE.

The half-cell efficiency (or cathodic EE) for CO production at each of the tested pressures and electrolytes is plotted in Fig. 3(d) (see SI for calculation description). The trends seen in this figure mirror closely those of the CO FE (Fig. 3(a)), indicating that the selectivity improvement was the primary driver of efficiency improvements. Still, overpotential has an influence on the energetic efficiency as the electrolyte concentration with the most selectivity is not necessarily the most efficient. At 1 atm, 1 M KOH electrolyte was the most efficient at 54.6%; however, as pressure is increased, the cathodic EE of the higher KOH conditions significantly outperforms the 1 M KOH case. Minimal changes in the cathodic EE were observed once the CO faradaic efficiency reached close to 100% and so further pressurization after this point offered little benefit (e.g. 5 M beyond 5 atm). Of all the conditions tested, the 7 M KOH at 7 atm demonstrated the highest half-cell EE for CO at 81.5%, representing a more than double improvement over its corresponding cathodic EE at 1 atm (38.9%) and a significant improvement over the highest cathodic EE at 1 atm (1 M KOH, 54.6%). Similarly, comparing the highest observed full cell EE (Fig. S8 (d)) of all the tested KOH electrolyte concentrations with pressure (40% in 7 M KOH at 7 atm) and without pressure (22% in 5 M KOH at 1 atm) we further illustrate the benefits of a system that is both pressurized and highly alkaline. Moreover, the benefits of the reduced electrical energy achieved through high pressurization and high alkalinity far outweigh the energy costs of pressurization (calculation in the SI) suggesting that such a reactor design may be advantageous even if a pressurized reactant stream is not available.

Comparison to other reports

The cathodic EE of our highest performing condition, 7 M at 7 atm, is compared to previously published reports of CO_2RR to CO at high current densities (>100 mA/cm^2) in Fig. 4(a) (citations for reports in Table S2).[12–17] We varied the current density applied to our Ag catalyst to report the EE at 200 mA/cm^2 (marked as 1a on the graph), 300 mA/cm^2 (marked as 1b on the graph), and 400 mA/cm^2 (marked as 1c on the graph). As can be observed in Fig. 4(a) the pressurized highly alkaline conditions in this report allows for the cathodic EE to be maintained above 80% for a range of high current densities, at least 10% higher than previous reports at similar current densities. In addition, when comparing to our highest EE condition at 1 atm in 1 M KOH (marked as 2 on the graph) to 7 atm in 7 M KOH (1b) at 300 mA/cm^2, the benefit of working under highly alkaline and pressurized conditions becomes more evident, with an increase in cathodic EE value of 50%.

Stability under CO_2RR conditions

While performance, in terms of cathodic and full cell EE is important, the stability of the catalyst is also crucial for commercial implementation. It is well-known that commercial carbon GDEs suffer from stability issues,[43] losing hydrophobicity and flooding over time. We observed that they show even worse behavior when subjected to pressure. To address this loss of hydrophobicity, we developed a new GDE similar to our prior report, that decouples the hydrophobic layer and current collector from the gas diffusion layer to markedly increase the stability of the GDE.[44] The Ag catalyst was sputter-deposited on this PTFE GDE (Fig S9) and operated for over 10 h at a cell potential of 2.8 V (non-iR corrected) in 7 M KOH at 7 atm (Fig. 4(b)). For the duration of the run, the catalyst remained very stable for CO generation displaying a FE between 85-90% for all collected gas samples. The FE for hydrogen remained low throughout the run (<2%), however it did increase slightly over time, which we believe is due to remaining electrolyte impurities depositing on the Ag catalyst over time. Moreover, the current remained stable between 80 to 100 mA/cm^2 throughout the run, with no degradation over time. We believe the difference in pore size and thickness of the PTFE GDE compared to the commercial carbon GDE affects gas diffusion through the GDE, and thus, we attribute the decrease in CO selectivity to a difference in the GDE structure and operation. The uninterrupted operation time in this system is an order of magnitude larger than those presented in literature for alkaline electrolyzers at much lower electrolyte concentrations and ambient pressures, [13,26] while also demonstrating the longest stable operation in a pressurized flow cell reported to date.[29,30]

While this new electrode structure is a major improvement in stability for alkaline electrolyzers compared to traditional carbon GDEs, it remains a challenge in this field to operate for very long time scales, 100s and 1000s of hours, while maintaining high selectivity and high current densities. Although we observed only a slight pH change of the electrolyte after running through the flow cell (14.78 to 14.77), the formation of bicarbonate/carbonate in alkaline electrolyzers is an issue that should be addressed in future work, perhaps through the optimization of the PTFE GDE pore structure to limit CO2 diffusion into the electrolyte. In addition to improving the GDE to operate under these industrially relevant conditions and eliminating bicarbonate/carbonate formation, future work will focus on reducing impurity deposition on the catalyst over time and exploring on-off cycling of the system to accommodate renewable energy sources.

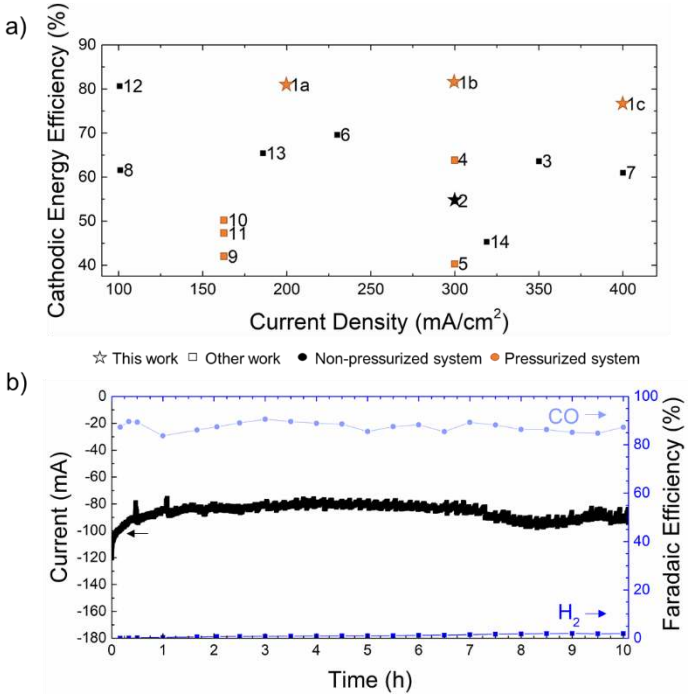

Fig 4.Performance of 7 M KOH at 7 atm. a) Comparison of cathodic EE to other high current density (>100 mA/cm^2) reports of CO_2RR to CO. All voltages reported are iR corrected based on reported values or from contact with the authors of the report, citations for each report in Table S2. b) Stability test of Ag catalyst in 7 M KOH at 7 atm at a full cell potential of 2.8V (non-iR corrected) and cathode area of 1 cm^2.

Conclusions

In summary, we report the benefits of the operation of CO_2RR catalysts under previously unexplored extreme alkaline conditions, including significantly reduced overpotentials necessary for CO_2RR onset and faster kinetics. However, these conditions caused an unwanted switch in selectivity from CO to formate production. By increasing the reaction pressure, we have discovered a method to improve CO selectivity while maintaining the benefits of the highly alkaline environment. It is through the combination of pressurization and highly alkaline reaction environments, the selectivity of CO_2RR-to-CO is maximized at overpotentials over 100 mV less than previous studies at similar current densities. We achieve the highest half-cell efficiency for CO production, 81.5%, at industrially relevant currents, 300 mA/cm^2. In addition, we demonstrate the high stability of such a system with a modified GDE design, capable of operating for over 10 hours under this extremely alkaline and pressurized system. This strategy of combining pressure with highly alkaline environments is well aligned with commercial systems and presents a feasible route to large scale CO_2RR implementation.

Experimental

Reagents

Potassium hydroxide (>85%), potassium chloride, and potassium iodide were purchased from Sigma Aldrich. All reagents were of analytical grade and were used without further purification. Milli-Q grade water (18.2 MΩ) was used to prepare all solutions.

Electrode Preparation

The cathode gas diffusion electrodes (GDEs) were prepared through the evaporation of 100nm of Ag (99.99%) using Angstron Nexdep Evaporator (~10^{-5}-10^{-6} Torr at 1.5 Å/sec) onto commercially available gas diffusion layers (Sigracet 39BC, Fuel Cell Store). Electrodes with Ag nanoparticles were fabricated through airbrushing the nanoparticle ink onto the commercial gas diffusion layers at a loading of 2 mg/cm^2, measured through weighing gas diffusion layer before and after spray coating. The nanoparticle ink was prepared by dispersing 100 mg of Ag nanoparticles (<100 nm particle size, Sigma-Aldrich) and 50 µl of Nafion Solution (Sigma-Aldrich) in 750 µl isopropyl alcohol and 250 µl of Milli-Q grade water (18.2 MΩ) and sonicated for 1 hour prior to air brushing.

Electrode Characterization

The Ag catalyst on the cathode GDE was characterized before and after CO_2RR. The cathode GDEs were characterized using Scanning Electron Microscopy (SEM) on a Hitachi S-5200 instrument (The Centre for Nanostructure Imaging, University of Toronto) apparatus and Transmission Electron Microscopy (TEM) on a Hitachi HF-3300 instrument (Ontario Centre for the Characterisation of Advanced Materials (OCCAM), University of Toronto) with an acceleration voltage of 300 kV. XAS measurements were recorded in fluorescence mode at the Ag K-edge (25510 eV), at the ROCK beamline of the SOLEIL synchrotron (France). The energy was calibrated against Ag foil. L3-edge XAS measurements were done at the Soft X-Ray Microcharacterization Beamline (SXRMB) at the Canadian Light Source (CLS). All normalization and analysis of the XAS data were performed using the Athena software. X-ray diffraction (XRD) were measured on a Philips X'Pert Pro Super X-ray diffractometer equipped with graphite-monochromatized Cu Ka radiation at the University of Toronto. X-ray photoelectron spectroscopy (XPS) was performed on an ESCALab MKII X-ray photoelectron spectrometer using Mg Ka radiation exciting source.

Operation of Electrochemical Flow Cell

All CO_2 reduction experiments were performed in an electrochemical flow cell configuration, as depicted in Fig. S1. The body of the flow cell was fabricated out of polytetrafluoroethylene (PTFE) with CO_2 gas and two liquid inlets, one for the catholyte and one for the anolyte. The cathode GDE prepared with catalyst (geometric active area of 1 or 2.25 cm^2) was separated from the anode by an anion exchange membrane (Fumatech FAA-3-PK-130). A nickel foam anode (MTI Corp. EQ-BCNF-80um) with a geometric surface area of 2.0 cm^2 was used as the anode. Liquid electrolyte (KOH) was introduced into the catholyte and anolyte chambers on each side of the anion exchange membrane. The distance between the cathode and anode was taken to be 9.5 mm. A reference Ag/AgCl (1 M KCl) electrode was mounted in a PTFE spacer in the catholyte stream at a fixed distance from the working electrode. Gaseous CO_2 was fed into the cell behind the cathode GDE and diffused into the liquid electrolyte present at the catalyst.

The CO_2 reduction experiments were performed using an electrochemical workstation (Autolab PGSTAT302N). The electrode potentials after iR compensation, resistance measured through electrochemical impedance spectroscopy (EIS) (Table S1), were rescaled to the reversible hydrogen electrode (RHE) reference by:

$$E_{RHE} = E_{Ag/AgCl} + 0.222\ V + 0.0591 \times pH$$

All CO_2 reduction experiments were performed under galvanostatic mode and the reported potentials were obtained by averaging over a timespan of at least 150 s for each applied current.

For each CO_2 reduction experiment, new electrolyte was prepared fresh and it was circulated through the electrochemical flow cell using peristaltic pumps at 10 mL min^{-1}. An automatic mass flow controller was used to maintain the flow of the input CO_2 (Linde, 99.99%) at 50 sccm throughout each experiment. The reactions were run for at least 150 s before the gas products were collected for analysis.

Product Analysis

The gas products from CO_2 reduction (CO, H_2) were analysed in 1 mL volumes using a gas chromatograph (PerkinElmer Clarus 680) coupled with a thermal conductivity detector (TCD) and a flame ionization detector (FID). The flow rate of the gas was measured before each 1mL volume was collected. The gas chromatograph was equipped with a Molecular Sieve 5A capillary column and a packed Carboxen-1000 column and argon (Linde, 99.999%) was used as the carrier gas.

The liquid products were quantified using nuclear magnetic resonance spectroscopy (NMR). 1H NMR spectra of freshly acquired samples were collected on Agilent DD2 500 spectrometer in 10% D_2O using water suppression mode, with Dimethyl sulfoxide (DMSO) as an internal standard. Sixteen second relaxation time between the pulses was used to allow for complete proton relaxation.

Pressure and Stability Testing

The CO_2 reduction experiments operated at higher pressures were carried out in a modified electrochemical flow cell, where the PTFE body was reinforced with aluminium end plates. This cell had a cathode active area of 1 cm^2 and an anode active area of 1.5 cm^2. The gas diffusion, cathode, and anode compartments had volumes of 0.51, 0.95, and 0.51 cm^3 respectively. There is some additional pressurized volume for each stream attributed to the tubing before and after the cell (PTFE tubing 3.18 mm outer diameter and 1.59 mm inner diameter).

A schematic of the pressure setup is shown in Fig. S6. The cell pressure was controlled using three back pressure regulators (BPRs, Equilibar model LF1 with PTFE glass laminate diaphragms) downstream of the cell. Teledyne Isco pumps were used to pump the catholyte and anolyte at flow rates of 2 and 1.5 mL min^{-1}, respectively. Transfer cells (High Pressure Equipment Co. model TOC-3-10-P) were used such that water from the pump would displace a piston inside the transfer cell, thereby forcing electrolyte out of the opposite end while protecting the pump from the electrolytes used in this experiment. Under this configuration, electrolyte was passed through the cell once, instead of re-circulated. The gas samples were collected downstream of the BPRs, ensuring that the gas is at atmospheric pressure. Similarly, to avoid any pressure effects on the reference electrode, the reference electrode was placed in the catholyte downstream of the BPR.

In order to avoid instabilities caused by the carbon gas diffusion layer during stability testing, a new electrode was developed, similar to our previous report, but without an additional carbon/graphite layer.[44] Briefly, a PTFE membrane with a pore size of 450 nm was sputtered with silver and used as the cathode. Stability tests were carried out using the same procedure as the pressure tests, except that they were operated potentiostatically under a full cell voltage of 2.8V. The current used for calculating FE was determined through averaging the current over the 50 seconds prior to the gas collection. Moreover, for the stability tests, the electrolyte was purified prior to be being introduced to the cell by passing a -10 mA current through it in a two electrode configuration using a GDE with Ag for the cathode and Pt foil for the anode for at least 0.5 hours.

Conflicts of interest

There are no conflicts to declare.

Acknowledgements

The authors acknowledge support from the Natural Sciences and Engineering Research Council (NSERC), the Government of Ontario through the Ontario Research Fund – Research Excellence program, and the Connaught Fund. X-ray spectroscopy measurements were performed at the Canadian Light Source (SXRMB beamline) and the authors thank Dr. Y. Hu and Dr. Q. Xiao for XAS support. The authors would like to thank Y. Wang, P. De Luna, D.-H. Nam, R.Q. Bermudez, and C.-S. Tan for their help with materials characterization. C.M.G. would like to thank NSERC for support in the form of a postdoctoral fellowship award. A.S. wishes to thank FRQNT for support in the form of postdoctoral fellowship award. J.P.E. thanks NSERC, Hatch and the Government of Ontario for their support through graduate scholarships. J.P.E. also thanks S. Verma and S. Bhargava at the Kenis Lab for helpful input on flow cell testing. T.B. thanks Hatch for a Graduate Scholarship for Sustainable Energy Research. M.K. acknowledges Banting postdoctoral fellowship from Govt. of Canada.

References

1 T. Sakakura, J. C. Choi and H. Yasuda, *Chem. Rev.*, 2007, **107**, 2365–2387.
2 H. Lin and E. J. Biddinger, *Energy Technol.*, 2017, **5**, 771–772.
3 C. Song, *Catal. Today*, 2006, **115**, 2–32.
4 P. J. A. Kenis, A. Dibenedetto and T. Zhang, *ChemPhysChem*, 2017, 3091–3093.
5 M. Bevilacqua, J. Filippi, H. A. Miller and F. Vizza, *Energy Technol.*, 2015, **3**, 197–210.
6 C. Oloman and H. Li, *ChemSusChem*, 2008, **1**, 385–391.

7 S. Verma, B. Kim, H. R. M. Jhong, S. Ma and P. J. A. Kenis, *ChemSusChem*, 2016, 1972–1979.
8 T. Haas, R. Krause, R. Weber, M. Demler and G. Schmid, *Nat. Catal.*, 2018, **1**, 32–39.
9 A. J. Martín, G. O. Larrazábal and J. Pérez-Ramírez, *Green Chem.*, 2015, **17**, 5114–5130.
10 M. Jouny, W. W. Luc and F. Jiao, *Ind. Eng. Chem. Res.*, 2018, **57**, 2165–2177.
11 X. Li, P. Anderson, H.-R. M. Jhong, M. Paster, J. F. Stubbins and P. J. A. Kenis, *Energy & Fuels*, 2016, **30**, 5980–5989.
12 S. Ma, R. Luo, J. I. Gold, A. Z. Yu and P. J. A. Kenis, *J. Mater. Chem. A*, 2016, **4**, 8573–8578.
13 S. Verma, Y. Hamasaki, C. Kim, W. Huang, S. Lu, H.-R. M. Jhong, A. A. Gewirth, T. Fujigaya, N. Nakashima and P. J. A. Kenis, *ACS Energy Lett.*, 2018, **3**, 193–198.
14 K. Hara and T. Sakata, *Bull. Chem. Soc. Jpn.*, 1997, **70**, 571–576.
15 S. Verma, X. Lu, S. Ma, R. I. Masel and P. J. A. Kenis, *Phys. Chem. Chem. Phys.*, 2016, **18**, 7075–7084.
16 S. Ma, Y. Lan, G. M. J. Perez, S. Moniri and P. J. A. Kenis, *ChemSusChem*, 2014, **7**, 866–874.
17 K. Hara, A. Kudo and T. Sakata, *J. Electroanal. Chem.*, 1995, **391**, 141–147.
18 D. T. Whipple and P. J. A. Kenis, *J. Phys. Chem. Lett.*, 2010, **1**, 3451–3458.
19 N.-T. Suen, S.-F. Hung, Q. Quan, N. Zhang, Y.-J. Xu and H. M. Chen, *Chem. Soc. Rev.*, 2017, **46**, 337–365.
20 X. Zheng, B. Zhang, P. De Luna, Y. Liang, R. Comin, O. Voznyy, L. Han, F. P. García de Arquer, M. Liu, C. T. Dinh, T. Regier, J. J. Dynes, S. He, H. L. Xin, H. Peng, D. Prendergast, X. Du and E. H. Sargent, *Nat. Chem.*, 2017, 2–7.
21 X. Xu, F. Song and X. Hu, *Nat. Commun.*, 2016, **7**, 1–7.
22 B. Zhang, Y. H. Lui, H. Ni and S. Hu, *Nano Energy*, 2017, **38**, 553–560.
23 J. Sun, H. Yin, P. Liu, Y. Wang, X. Yao, Z. Tang and H. Zhao, *Chem. Sci.*, 2016, **7**, 5640–5646.
24 X. Lu, W. L. Yim, B. H. R. Suryanto and C. Zhao, *J. Am. Chem. Soc.*, 2015, **137**, 2901–2907.
25 F. Song and X. Hu, *Nat. Commun.*, 2014, **5**, 1–9.
26 B. Endrődi, G. Bencsik, F. Darvas, R. Jones, K. Rajeshwar and C. Janáky, *Prog. Energy Combust. Sci.*, 2017, **62**, 133–154.
27 Q. Lu and F. Jiao, *Nano Energy*, 2016, **29**, 439–456.
28 S. Ma, M. Sadakiyo, R. Luo, M. Heima, M. Yamauchi and P. J. A. Kenis, *J. Power Sources*, 2016, **301**, 219–228.
29 E. J. Dufek, T. E. Lister, S. G. Stone and M. E. McIlwain, *J. Electrochem. Soc.*, 2012, **159**, F514–F517.
30 E. J. Dufek, T. E. Lister and S. G. Stone, *J. Appl. Electrochem.*, 2014, **44**, 849–855.
31 M. E. Boot-Handford, J. C. Abanades, E. J. Anthony, M. J. Blunt, S. Brandani, N. Mac Dowell, J. R. Fernández, M.-C. Ferrari, R. Gross, J. P. Hallett, R. S. Haszeldine, P. Heptonstall, A. Lyngfelt, Z. Makuch, E. Mangano, R. T. J. Porter, M. Pourkashanian, G. T. Rochelle, N. Shah, J. G. Yao and P. S. Fennell, *Energy Environ. Sci.*, 2014, **7**, 130–189.
32 M. K. Chandel, L. F. Pratson and E. Williams, *Energy Convers. Manag.*, 2010, **51**, 2825–2834.
33 H. Krässig, J. Schurz, R. G. Steadman, K. Schliefer, W. Albrecht, M. Mohring and H. Schlosser, in *Ullmann's encyclopedia of industrial chemistry Vol.6*, 2012, pp. 679–693.
34 V. Subramani and S. K. Gangwal, *Energy & Fuels*, 2008, **22**, 814–839.
35 K. Fang, D. Li, M. Lin, M. Xiang, W. Wei and Y. Sun, *Catal. Today*, 2009, **147**, 133–138.
36 P. De Luna, R. Quintero-Bermudez, C.-T. Dinh, M. B. Ross, O. S. Bushuyev, P. Todorović, T. Regier, S. O. Kelley, P. Yang and E. H. Sargent, *Nat. Catal.*, 2018, **1**, 103–110.
37 A. Seifitokaldani, C. M. Gabardo, T. Burdyny, C.-T. Dinh, J. P. Edwards, M. G. Kibria, O. S. Bushuyev, S. O. Kelley, D. Sinton and E. H. Sargent, *J. Am. Chem. Soc.*, 2018, **140**, 3833–3837.
38 C. M. Gunathunge, V. J. Ovalle and M. M. Waegele, *Phys. Chem. Chem. Phys.*, 2017, **19**, 30166–30172.
39 K. P. Kuhl, E. R. Cave, D. N. Abram and T. F. Jaramillo, *Energy Environ. Sci.*, 2012, **5**, 7050.
40 J. Rosen, G. S. Hutchings, Q. Lu, S. Rivera, Y. Zhou, D. G. Vlachos and F. Jiao, *ACS Catal.*, 2015, **5**, 4293–4299.
41 C. Amatore and J. M. Savéant, *J. Am. Chem. Soc.*, 1981, **103**, 5021–5023.
42 A. Gennaro, A. A. Isse, M.-G. Severin, E. Vianello, I. Bhugun and J.-M. Savéant, *J. Chem. Soc., Faraday Trans.*, 1996, **92**, 3963–3968.
43 J. Park, H. Oh, T. Ha, Y. Il and K. Min, *Appl. Energy*, 2015, **155**, 866–880.
44 C.-T. Dinh, T. Burdyny, G. Kibria, A. Seifitokaldani, C. M. Gabardo, F. P. G. de Arquer, A. Kiani, J. P. Edwards, P. De Luna, O. S. Bushuyev, C. Zou, R. Quintero-Bermudez, Y. Pang, D. Sinton and E. H. Sargent, *Science (80-.).*, 2018, **360**, 783–787.